ACS OMEGA

Open Access



http://pubs.acs.org/journal/acsodf

Article

# A Comparative DFT Investigation of the Adsorption of Temozolomide Anticancer Drug over Beryllium Oxide and Boron Nitride Nanocarriers

Mahmoud A. A. Ibrahim,* Al-Shimaa S. M. Rady, Peter A. Sidhom, Shaban R. M. Sayed, Khalid Elfaki Ibrahim, Ahmed M. Awad, Tamer Shoeib,* and Lamiaa A. Mohamed

Cite This: *ACS Omega* 2024, 9, 25203−25214

Read Online

ACCESS | Metrics & More | Article Recommendations | Supporting Information

**ABSTRACT:** Herein, attempts were made to explore the adsorption prospective of beryllium oxide ($Be_{12}O_{12}$) and boron nitride ($B_{12}N_{12}$) nanocarriers toward the temozolomide (TMZ) anticancer drug. A systematic investigation of the TMZ adsorption over nanocarriers was performed by using quantum chemical density functional theory (DFT). The favorability of $Be_{12}O_{12}$ and $B_{12}N_{12}$ nanocarriers toward loading TMZ was investigated through A↔D configurations. Substantial energetic features of the proposed configurations were confirmed by negative adsorption ($E_{ads}$) energy values of up to −30.47 and −26.94 kcal/mol for TMZ•••$Be_{12}O_{12}$ and •••$B_{12}N_{12}$ complexes within configuration A, respectively. As per SAPT results, the dominant contribution beyond the studied adsorptions was found for the electrostatic forces ($E_{elst}$ = −100.21 and −63.60 kcal/mol for TMZ•••$B_{12}N_{12}$ and •••$Be_{12}O_{12}$ complexes within configuration A, respectively). As a result of TMZ adsorption, changes in the energy of molecular orbitals followed by alterations in global reactivity descriptors were observed. Various intermolecular interactions within the studied complexes were assessed by QTAIM analysis. Notably, a favorable adsorption process was also observed under the effect of water with adsorption energy ($E_{ads}^{solvent}$) reaching −28.05 and −22.26 kcal/mol for TMZ•••$B_{12}N_{12}$ and •••$Be_{12}O_{12}$ complexes within configuration A, respectively. The drug adsorption efficiency of the studied nanocarriers was further examined by analyzing the IR and Raman spectra. From a sustained drug delivery point of view, the release pattern of TMZ from the nanocarrier surface was investigated by recovery time calculations. Additionally, the significant role of doping by heavy atoms (i.e., $MgBe_{11}O_{12}$ and $AlB_{11}N_{12}$) on the favorability of TMZ adsorption was investigated and compared to pure analogs (i.e., $Be_{12}O_{12}$ and $B_{12}N_{12}$). The obtained data from thermodynamic calculations highlighted that the adsorption process over pure and doped nanocarriers was spontaneous and exothermic. The emerging findings provide a theoretical base for future works related to nanocarrier applications in the drug delivery process, especially for the TMZ anticancer drug.

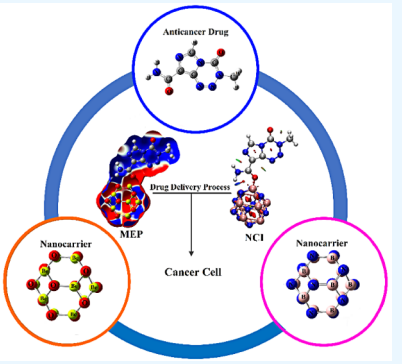


## INTRODUCTION

Nanotechnology, first proposed in 1965, has piqued significant interest due to its applications in various life sectors.[1−4] With the advent of nanotechnology, numerous strategies have been introduced toward targeted drug delivery processes.[5−7] Consequently, nanoscale materials (i.e., nanocarriers) have been applied as targeted and controlled drug delivery systems.[8,9] Nanocarriers are characterized as one of the foremost promising drug delivery systems with boundless possibilities. Nanocarriers are anticipated to enhance the solubility of drugs within the body.[10,11] Due to their small size, nanocarriers are able to easily penetrate the cell barrier and deliver drugs in significant concentration.[12] Besides, nanocarriers show promising properties such as good biocompatibility and high drug-loading capacity.[13,14] Fullerene and fullerene-like nanocarriers have theoretically been applied in the drug delivery process.[15,16] Indeed, symmetrical metal oxides (i.e., $Mg_{12}O_{12}$, $Be_{12}O_{12}$, and $Zn_{12}O_{12}$) have attracted attention due to their unique properties related to the ionic character of metal oxide bonds.[17] According to the literature, the adsorption performance of metal oxides toward various drugs was investigated.[18] For instance, the favorable adsorption process of favipiravir over metal oxides was conducted using DFT calculations.[19] As potent drug delivery systems, the adsorption process of isoniazid anticancer drug over metal oxides was elucidated.[20] Of interest, $Be_{12}O_{12}$ was proposed to be thermally stable, promoting its application as a drug delivery system for several drugs.[21,22]

Received: March 25, 2024
Revised: May 14, 2024
Accepted: May 17, 2024
Published: May 30, 2024

On the contrary, boron nitride ($B_xN_x$ where $x$ identifies the number of B and N atoms) nanocarriers have exceptional features permitting their use in the drug delivery process.[23,24] Notably, $B_xN_x$ nanocarriers have been reported to be nontoxic, leading them to be suitable for biomedical applications.[25] Among $B_xN_x$ structures, $B_{12}N_{12}$ was introduced as a prominent nanocarrier and applied in the drug delivery process.[26] By means of DFT, $B_{12}N_{12}$ was widely examined as a potent delivery system for anticancer and anti−COVID-19 drugs.[27−29]

The adsorption properties of nanocarriers could be changed by means of the doping process.[30] In this respect, doping foreign atoms to nanocarriers substantially enhanced the adsorption potential.[31,32] In more detail, the applicability of $B_{24}N_{24}$ and Al- and Ga-doped $B_{24}N_{24}$ nanocarriers in the delivery process for lomustine anticancer drug was investigated, demonstrating that the Al-doped $B_{24}N_{24}$ is the most preferable system.[33] In this regard, the tendency of $B_{12}N_{12}$ as well as $AlB_{11}N_{12}$ and $GaB_{11}N_{12}$ nanocarriers toward 5-aminosalicylic Acid (5-ASA) drug adsorption was examined, ensuring the enhancing role of the doped nanocarriers.[34] On the basis of DFT calculations, the favorable role of the $AlB_{11}N_{12}$ nanocarrier in the delivery process of chlormethine (CM) anticancer drug was demonstrated.[35]

Temozolomide (TMZ) is an oral chemotherapeutic agent with the molecular formula of $C_6H_6N_6O_2$.[36] TMZ was approved for treating anaplastic astrocytoma and gliomas (brain tumors).[37] However, TMZ has many side effects, including nausea, headaches, and rashes. Essentially, the side effects of drugs can be minimized by applying nanocarriers that deliver drugs with specific concentrations to a limited number of cells without affecting other cells. In that spirit, the drug delivery process for TMZ was investigated by employing fullerene-like nanocarriers.[38,39]

According to the literature, the potential of $Be_{12}O_{12}$ as a drug delivery system for TMZ anticancer drugs has not been reported yet. Thus, the tendency of $Be_{12}O_{12}$ toward adsorbing TMZ anticancer drug was thoroughly elucidated and comparatively addressed with the $B_{12}N_{12}$ analog for the first time. Toward addressing the occurrence and favorability of the adsorption process, TMZ•••$Be_{12}O_{12}$ and •••$B_{12}N_{12}$ complexes were examined within different orientations (see Figure 1). Subsequently, geometrical optimization and frequency calculations were performed, followed by electrostatic potential (ESP) analysis. Furthermore, symmetry-adapted perturbation theory (SAPT) and noncovalent interaction (NCI) index, along with quantum theory of atoms in molecules (QTAIM), were analyzed. From an electronic perspective, frontier molecular orbital (FMO) theory was applied, and global reactivity descriptors were calculated. To further illustrate this, infrared (IR) spectra, conjointly with Raman, were extracted for the studied nanocarriers before and after TMZ adsorption. The drug desorption was simulated by calculating the recovery time for the studied complexes. Furthermore, the role of the doping strategy in the adsorption process was evaluated by studying the TMZ•••$MgBe_{11}O_{12}$ and •••$AlB_{11}N_{12}$ complexes. The current work aims to introduce an effective nanocarrier with potential applications in the drug delivery process, specifically for the TMZ anticancer drug.

## COMPUTATIONAL METHODS

In the context of quantum chemical calculations, $Be_{12}O_{12}$ and $B_{12}N_{12}$ nanocarriers were comparatively examined to adsorb the TMZ anticancer drug. Within the framework of Gaussian 09,[40] the DFT/M06-2X method in tandem with 6−311+G** basis set[41] was applied for all performed calculations. Initially, geometrical optimization was performed for the TMZ, $Be_{12}O_{12}$, and $B_{12}N_{12}$ molecular structures. Following that, frequency calculations were executed to confirm that the optimized geometries are true minima. According to the geometries obtained, an electrostatic potential (ESP) analysis was performed to illustrate the different potentials over the molecular surfaces. A detailed illustration from ESP was given by generating the maps of molecular electrostatic potential (MEP), at an electron density envelope of 0.002 au.[42] By using Multiwfn 3.7 software,[43] the numerical description of MEP maps was obtained by means of electrostatic potential extrema ($V_{s,max/min}$) values. Toward the drug-loading process, the TMZ•••$Be_{12}O_{12}$ and •••$B_{12}N_{12}$ complexes were examined through various configurations (see Figure 1). All studied geometries were optimized at the M06−2X/6−311+G** level of theory. Based on the most stable structures, the doping process by Mg and Al atoms was applied to $Be_{12}O_{12}$ and $B_{12}N_{12}$ nanocarriers, forming TMZ•••$MgBe_{11}O_{12}$ and •••$AlB_{11}N_{12}$ complexes, respectively. For proficient adsorption within the optimized complexes, adsorption ($E_{ads}$) energies were calculated. Within the realm of energy calculations, the counterpoise procedure (CC), advocated by Boys and Bernardi,[44] was taken into account to remove the basis set superposition error (BSSE), as follows:

$$E_{ads} = E_{TMZ\cdots nanocarrier} - (E_{TMZ} + E_{nanocarrier}) + E_{BSSE} \quad (1)$$

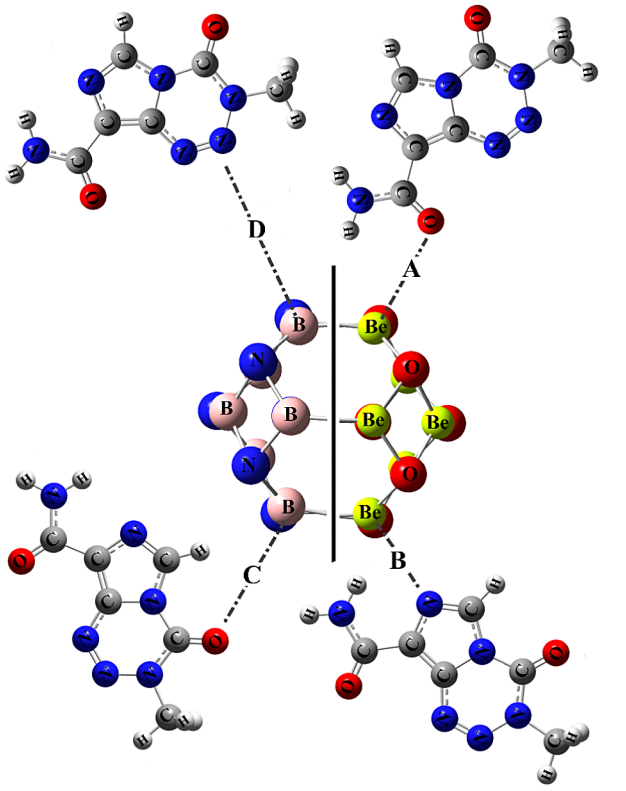


**Figure 1.** Illustration showing the adsorption of the temozolomide (TMZ) anticancer drug with $Be_{12}O_{12}$ and $B_{12}N_{12}$ nanocarriers within four orientations labeled from A to D.



https://doi.org/10.1021/acsomega.4c02882
ACS Omega 2024, 9, 25203−25214

where the energies of studied complexes, isolated TMZ, and isolated nanocarriers were represented by $E_{TMZ•••nanocarrier}$, $E_{TMZ}$, and $E_{nanocarrier}$, respectively.

To glean an insightful perspective on the contribution of physical forces within the adsorption process, symmetry-adapted perturbation theory (SAPT) analysis was employed. SAPT analysis was performed with the help of PSI4 package[45] at the SAPT0 level. Accordingly, total SAPT0 and its four physical components—namely, electrostatic, dispersion, induction, and exchange were calculated as follows:

$$E^{SAPT0} = E_{elst} + E_{disp} + E_{ind} + E_{exch} \quad (2)$$

where:

$$E_{elst} = E_{elst}^{(10)} \quad (3)$$

$$E_{disp} = E_{disp}^{(20)} + E_{exch-disp}^{(20)} \quad (4)$$

$$E_{ind} = E_{ind,\,resp}^{(20)} + E_{exch-ind,\,resp}^{(20)} + \delta E_{HF,\,resp}^{(2)} \quad (5)$$

$$E_{exch} = E_{exch}^{(10)} \quad (6)$$

where $E^{SAPT0}$, $E_{elst}$, $E_{disp}$, $E_{ind}$, and $E_{exch}$ identify total SAPT0, electrostatic, dispersion, induction, and exchange, respectively. For insightful bonding features among the considered systems, the quantum theory of atoms in molecules (QTAIM) combined with noncovalent interaction (NCI) index analyses were conducted. From QTAIM descriptions, bond paths (BPs) and bond critical points (BCPs) were generated between the interacted systems. Meanwhile, topological parameters such as electron density ($\rho_b$), kinetic electron density ($G_b$), total energy density ($H_b$), local potential electron energy density ($V_b$), Laplacian ($\nabla^2\rho_b$), and the negative ratio of kinetic and potential electron energy density ($-G_b/V_b$) were calculated. Inspired by NCI, 3D diagrams were generated and displayed with colored scale according to $(\lambda_2)\rho$ values from −0.035 au (blue) to 0.020 au (red). Indeed, QTAIM and NCI analyses were performed using Multiwfn 3.7 software.[43] Furthermore, the visualization was conducted by the Visual Molecular Dynamics (VMD) program.[46]

By means of electronic properties, the investigated adsorption process was examined from a frontier molecular orbitals (FMO) theory point of view. In the essence of FMOs, the patterns of molecular orbitals containing the highest-occupied molecular orbital (HOMO) and lowest-unoccupied molecular orbital (LUMO) were mapped, and their energies were estimated. Consequently, the LUMO−HOMO energy gap ($E_{gap}$) and the Fermi level ($E_{FL}$) energies were calculated based on the $E_{HOMO}$ and $E_{LUMO}$ energies, as shown in the following equations:

$$E_{gap} = E_{LUMO} - E_{HOMO} \quad (7)$$

$$E_{FL} = E_{HOMO} + \frac{E_{LUMO} - E_{HOMO}}{2} \quad (8)$$

From the $E_{HOMO}$ and $E_{LUMO}$ values, molecular reactivity indicators were calculated for TMZ, nanocarriers, and complexes. Consequently, the ionization potential ($IP$), electron affinity ($EA$), global hardness ($\eta$), global softness ($S$), electrophilicity index ($\omega$), chemical potential ($\mu$), and work function ($\Phi$) parameters can be calculated as follows:

$$IP \approx -E_{HOMO} \quad (9)$$

$$EA \approx -E_{LUMO} \quad (10)$$

$$\eta = \frac{E_{LUMO} - E_{HOMO}}{2} \quad (11)$$

$$s = \frac{1}{\eta} \quad (12)$$

$$\omega = \frac{\mu^2}{2\eta} \quad (13)$$

$$\mu = \frac{E_{LUMO} + E_{HOMO}}{2} \quad (14)$$

$$\Phi = V_{eL(+\infty)} - E_{FL} \quad (15)$$

Within eq 15, the $V_{eL}(+\infty)$ characterizes the vacuum-level electrostatic potential (where $V_{el}(+\infty) \approx 0$). From another avenue, the favorable adsorbing behavior of the investigated nanocarriers was examined using electrical conductivity ($\sigma$) that can be calculated as follows:

$$\sigma\alpha \mathrm{Exp}\left(\frac{-E_{gap}}{kT}\right) \quad (16)$$

As described above, the energy gap is represented by $E_{gap}$, the temperature is termed by T, and the Boltzmann's constant is defined by k. Toward a descriptive electronic glance, the plots of the density of states (TDOS and PDOS) were visualized with the help of GaussSum software.[47] Moreover, the adsorption process was examined in the presence of a water solvent by applying the polarizable continuum model (PCM). Considering the PCM method, the structures under investigation were optimized at a level of theory similar to that in the gas state. Thence, the adsorption ($E_{ads}^{solvent}$) energies were calculated for all considered complexes in the water. In the scope of the total energies, solvation ($\Delta E_{solv}$) energies were computed, as explained in the following formula:

$$\Delta E_{solv} = E_{solvent} - E_{gas} \quad (17)$$

where $E_{solvent}$ and $E_{gas}$ represent the total energy in the solvent phase and gas phase, respectively. Moreover, the interactions within the studied complexes were examined by means of thermodynamic parameters. Gibbs free energy ($\Delta G$), enthalpy ($\Delta H$), and entropy ($\Delta S$) were calculated by the following equations:

$$\Delta M = M_{TMZ\cdots nanocarrier} - (M_{TMZ} + M_{nanocarrier}) + E_{BSSE} \quad (18)$$

$$\Delta S = -(\Delta G - \Delta H)/T \quad (19)$$

As explained in the above formula, $\Delta M$ refers to the $\Delta G$ and $\Delta H$ energies for the optimized complexes. Besides, $M_{TMZ•••nanocarrier}$, $M_{TMZ}$, and $M_{nanocarrier}$ define the $G/H$ parameters of the optimized complexes, TMZ, and nanocarriers, respectively. Finally, the tendency of TMZ to separate from nanocarriers was elucidated by recovery time ($\tau$) calculation as follows:

$$t = \nu^{-1}\exp(-\Delta G/KT) \quad (20)$$

The attempt frequency ($10^{-18}$ $s^{-1}$) and Boltzmann's constant (0.00199 kcal/mol.K) are given as $\nu^{-1}$ and k, respectively.[34] The temperature is represented by T with


https://doi.org/10.1021/acsomega.4c02882
ACS Omega 2024, 9, 25203−25214

values of 298.15 (in the room), 310.15 (for the human body), and 315.15 K (for cancer cells).

## RESULTS AND DISCUSSION

**ESP Analysis.** Electrostatic potential (ESP) is straightforward in predicting the preferred adsorption sites for the drug delivery process.[48] ESP analysis was conducted for TMZ, $Be_{12}O_{12}$, and $B_{12}N_{12}$ optimized structures. Molecular electrostatic potential (MEP) surfaces were then plotted and supported by the $V_{s,max}$ and $V_{s,min}$ values (kcal/mol), as presented in Figure 2.

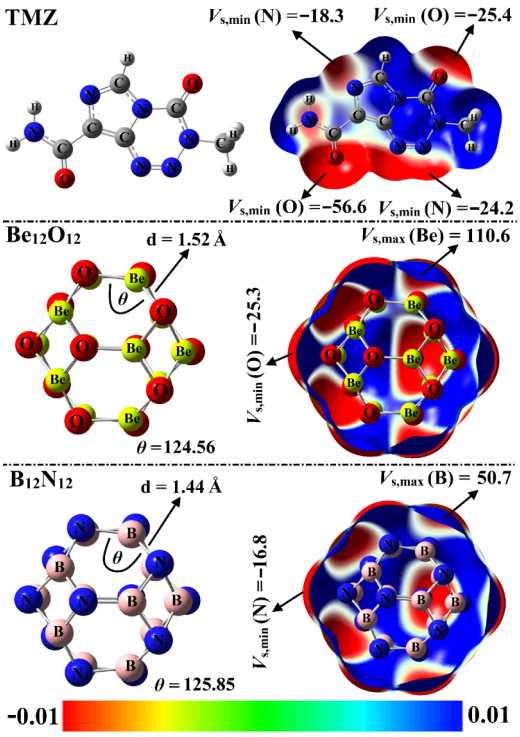


**Figure 2.** An overview showing the optimum geometries for TMZ, $Be_{12}O_{12}$, and $B_{12}N_{12}$ systems combined with MEP maps with color scale (from −0.01 (red) to +0.01 (blue) au) and the calculated $V_{s,max}$/$V_{s,min}$ values (kcal/mol).

Figure 2 depicts the geometrical structures of optimized $Be_{12}O_{12}$ and $B_{12}N_{12}$, comprising eight hexagonal and six tetragonal rings. In this regard, it was found that Be−O (B−N) bond lengths exhibited 1.52 (1.44) Å and 1.57 (1.48) Å between 6-6 and 6−4 membered rings, respectively. Notably, the obtained Be−O and B−N bond lengths were endorsed by previous studies.[18,49]

According to the relevant MEP maps, various charge accumulation sites (i.e., red regions) were observed along the molecular surface of the TMZ. Identifying these red regions, negative $V_{s,min}$ values were observed, ranging from −18.3 to −56.6 kcal/mol. Besides, substantial electron depletion regions (i.e., blue regions) were noticed for Be and B atoms in $Be_{12}O_{12}$ and $B_{12}N_{12}$ nanocarriers, which were numerically found with $V_{s,max}$ values of 110.6 and 50.7 kcal/mol, respectively. According to these observations, a favorable drug adsorption process could be predicted between the TMZ drug and the selected nanocarriers through different adsorption sites.

**Adsorption Process.** The promising drug-loading prospective of $Be_{12}O_{12}$ and $B_{12}N_{12}$ nanocarriers toward the TMZ drug was investigated. As a consequence, geometrical optimization was performed for configuration A↔D. The optimized structures for the most favorable configurations are depicted in Figure 3. From an energy perspective, adsorption ($E_{ads}$) energy values were computed and are collected in Table 1.

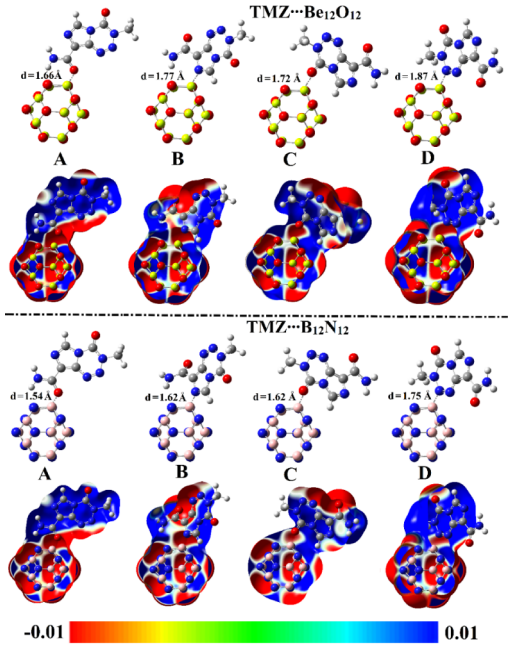


**Figure 3.** Optimized TMZ●●●nanocarrier complexes and MEP maps with color scale −0.01 au (red) to +0.01 au (blue) for configurations A↔D. The separation distances (d) are in Å.

**Table 1. Adsorption Energy ($E_{ads}$, kcal/mol) and Minimum Distances (d, Å) for the Optimized TMZ●●●Nanocarrier Complexes**

| complex | configuration | d | $E_{ads}$ |
|---|---|---|---|
| TMZ●●●$Be_{12}O_{12}$ | A | 1.66 | −30.47 |
| | B | 1.77 | −26.67 |
| | C | 1.72 | −18.26 |
| | D | 1.87 | −15.12 |
| TMZ●●●$B_{12}N_{12}$ | A | 1.54 | −26.94 |
| | B | 1.62 | −24.72 |
| | C | 1.62 | −11.12 |
| | D | 1.75 | −9.76 |

As listed in Table 1, the absorption of TMZ over the surfaces of $Be_{12}O_{12}$ and $B_{12}N_{12}$ was verified through substantial $E_{ads}$ values. The adsorption process within TMZ●●●$Be_{12}O_{12}$ and ●●●$B_{12}N_{12}$ complexes was further ensured through short adsorption distances from 1.87 to 1.54 Å (see Figure 3 and Table 1). Numerically, configuration A had energetic values higher than those of the others, and the overall $E_{ads}$ values decreased in the following order: A > B > C > D. By considering all investigated complexes, TMZ●●●$Be_{12}O_{12}$ complexes exhibited more negative $E_{ads}$ values compared to TMZ●●●$B_{12}N_{12}$ counterparts. For instance, configuration A had $E_{ads}$ values of −30.47 and −26.94 kcal/mol for the TMZ●●●$Be_{12}O_{12}$ and ●●●$B_{12}N_{12}$ complexes, respectively. The preferential adsorbing ability of the $Be_{12}O_{12}$ nanocarrier could be attributed to the higher electrophilic and nucleophilic


https://doi.org/10.1021/acsomega.4c02882
ACS Omega 2024, 9, 25203−25214

Table 2. Obtained Values of Total SAPT0 ($E^{SAPT0}$), Electrostatic ($E_{elst}$), Dispersion ($E_{disp}$), Induction ($E_{ind}$), and Exchange ($E_{exch}$) Energies (kcal/mol) for the Optimized Complexes

| complex | configuration | $E^{SAPT0}$ | $E_{elst}$ | $E_{disp}$ | $E_{ind}$ | $E_{exch}$ |
|---|---|---|---|---|---|---|
| TMZ•••$Be_{12}O_{12}$ | A | −46.86 | −63.60 | −12.74 | −30.70 | 60.19 |
| | B | −38.76 | −61.76 | −16.19 | −24.77 | 63.96 |
| | C | −30.07 | −40.17 | −14.43 | −21.08 | 45.60 |
| | D | −21.77 | −32.84 | −13.44 | −17.17 | 41.69 |
| TMZ•••$B_{12}N_{12}$ | A | −50.93 | −100.21 | −24.73 | −65.59 | 139.60 |
| | B | −41.31 | −104.62 | −30.34 | −53.73 | 147.37 |
| | C | −32.86 | −68.08 | −25.79 | −48.47 | 109.49 |
| | D | −23.51 | −60.97 | −25.16 | −39.37 | 102.00 |

nature of the Be and O atoms in $Be_{12}O_{12}$ compared to the B and N atoms in $B_{12}N_{12}$, respectively (see ESP results). Overall, substantial energy values affirmed the favorability of the investigated adsorption process, where $Be_{12}O_{12}$ and $B_{12}N_{12}$ could be potent nanocarriers for the TMZ drug delivery process.

**SAPT Calculations.** In an attempt to reliably estimate the specific contribution of physical forces within the TMZ•••$Be_{12}O_{12}$ and •••$B_{12}N_{12}$ complexes, symmetry-adapted perturbation theory (SAPT) analysis was applied. For the investigated complexes, the total SAPT0 energies with their four components were calculated and are summarized in Table 2.

In Table 2, significant negative values of total SAPT0 ($E^{SAPT0}$) affirmed the occurrence of the adsorption process within the TMZ•••$Be_{12}O_{12}$ and •••$B_{12}N_{12}$ complexes. In that spirit, favorable contributions were found for electrostatic ($E_{elst}$) forces combined with dispersion ($E_{disp}$) and induction ($E_{ind}$) forces that are illustrated by negative values. Contrarily, an unfavorable role was found for the exchange ($E_{exch}$) forces. For instance, the $E_{elst}$, $E_{disp}$, $E_{ind}$, and $E_{exch}$ values were found to be −63.60, − 12.74, − 30.70, and 60.19 kcal/mol for the TMZ•••$Be_{12}O_{12}$ complex within configuration A, respectively.

**QTAIM and NCI Calculations.** For insightful perspectives about the character and intensity of interactions within the considered complexes, the quantum theory of atoms in molecules (QTAIM) analysis was applied. Furthermore, QTAIM offered bonding insights through drawing bond paths (BPs) and bond critical points (BCPs) along with calculating the topological characteristics for a drug delivery process.[50] Accompanied by QTAIM, the noncovalent interaction (NCI) index was further performed for the studied complexes.[51] According to NCI index analysis, 2D NCI spikes were extracted for all considered configurations (Figure S1). By considering NCI index analysis, 3D colored plots were generated with a 0.50 au value of the reduced density gradient and colored from blue to red according to sign($\lambda_2$)$\rho$. For all investigated complexes, molecular graphs of QTAIM and 3D NCI were extracted and are depicted in Figure 4. Moreover, QTAIM topological features for the optimized TMZ•••nanocarrier complexes are listed in Table 3.

Figure 4 gives a meaningful illustration of the occurrence and nature of the interactions within the studied complexes, attributed to the presence of versatile bond paths (BPs) connecting the TMZ (i.e., the O and N atoms) with nanocarriers (i.e., the Be and B atoms). It was clear to observe the contribution of secondary interactions that also were noticed with the formation of bond critical points (BCPs) paired with bond paths (BPs) between H atoms of TMZ and O/N atoms of nanocarriers (Figure 4). The above-mentioned

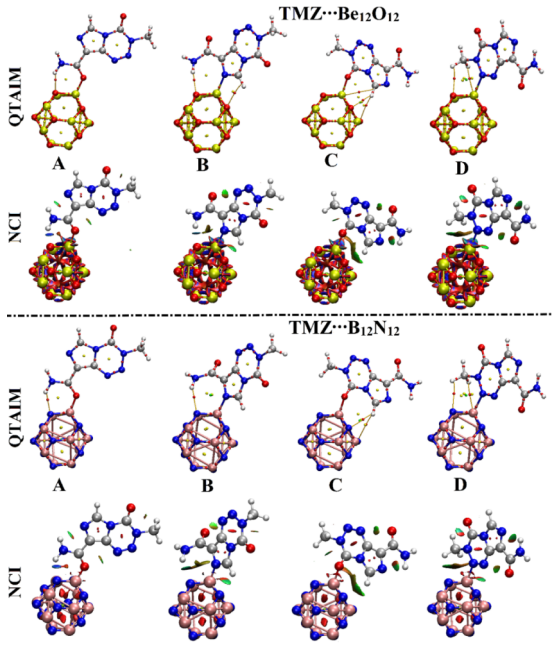


Figure 4. QTAIM and NCI molecular graphs for the optimized TMZ•••nanocarrier complexes within configurations A↔D.

observations strongly affirmed the tendency of $Be_{12}O_{12}$ and $B_{12}N_{12}$ toward adsorbing TMZ. Turning to NCI isosurfaces, the adsorption process was further buttressed via colored isosurfaces between adsorbed species. In this regard, the colored scale of isosurfaces aligned with the adsorption strength, where the blue and green colors indicated strong and weak interactions, respectively. Similar to 3D NCI results, 2D NCI spikes also affirmed the attractive interactions among the studied complexes (Figure S1).

According to the data in Table 3, the positive values of $\nabla^2\rho_b$ and negative values of $H_b$, along with values less than the unity of $-G_b/V_b$, highlighted the electrostatic and partial covalent interactions within TMZ•••$Be_{12}O_{12}$ and •••$B_{12}N_{12}$ complexes. For example, the $\nabla^2\rho_b$, $H_b$, and $-G_b/V_b$ of TMZ•••$B_{12}N_{12}$ within configuration A were found with values of 0.5173, − 0.0654, and 0.7486 au, respectively.

**Electronic Parameters.** Within the realm of electronic features, the frontier molecular orbitals (FMO) theory was invoked for the investigated drug adsorption process within all complexes.[52] According to the FMO theory, the HOMO and LUMO distributions were mapped for the isolated systems and TMZ•••nanocarrier complexes in Figures 5,6, respectively. Furthermore, the $E_{HOMO}$, $E_{LUMO}$, $E_{gap}$, and $E_{FL}$ values were calculated and are gathered in Table 4.



https://doi.org/10.1021/acsomega.4c02882
ACS Omega 2024, 9, 25203−25214

Table 3. QTAIM Topological Features (Given in au) for the Optimized TMZ•••Nanocarrier Complexes

| complex | configuration | $\rho_b$ | $G_b$ | $H_b$ | $V_b$ | $\nabla^2\rho_b$ | $-G_b/V_b$ |
|---|---|---|---|---|---|---|---|
| TMZ•••$Be_{12}O_{12}$ | A | 0.0628 | 0.1117 | 0.0047 | −0.1070 | 0.4654 | 1.0437 |
| | B | 0.0558 | 0.0845 | −0.0019 | −0.0864 | 0.3302 | 0.9778 |
| | C | 0.0499 | 0.0880 | 0.0065 | −0.0815 | 0.3782 | 1.0798 |
| | D | 0.0419 | 0.0623 | 0.0014 | −0.0609 | 0.2549 | 1.0230 |
| TMZ•••$B_{12}N_{12}$ | A | 0.1160 | 0.1947 | −0.0654 | −0.2601 | 0.5173 | 0.7486 |
| | B | 0.1164 | 0.1620 | −0.0796 | −0.2416 | 0.3296 | 0.6705 |
| | C | 0.0084 | 0.0058 | 0.0013 | −0.0045 | 0.0284 | 1.2867 |
| | D | 0.1925 | 0.1024 | −0.0543 | −0.1568 | 0.0854 | 0.6535 |

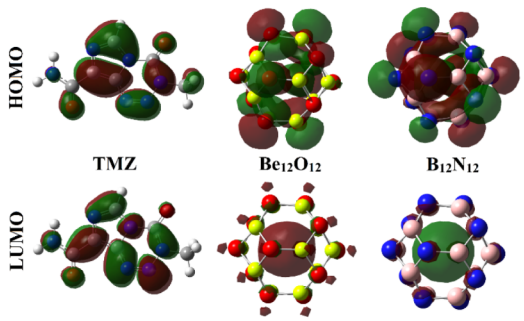


Figure 5. Patterns of HOMO and LUMO for the optimized TMZ, $Be_{12}O_{12}$, and $B_{12}N_{12}$ systems.

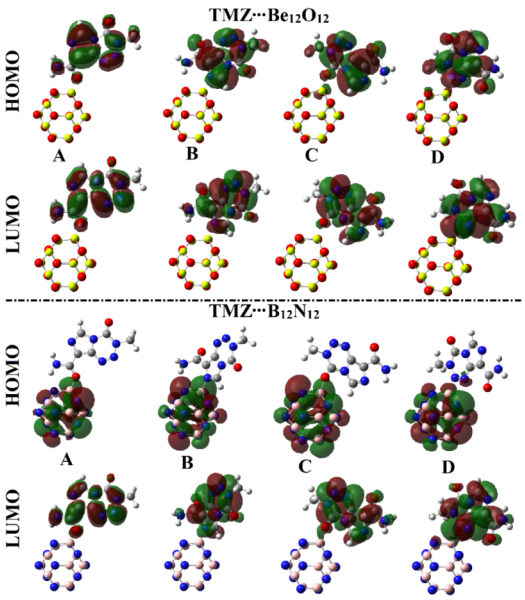


Figure 6. Patterns of HOMO and LUMO for the optimized TMZ•••nanocarrier complexes within configurations A↔D.

As illustrated in Figure 5, HOMO levels were mainly confined over the nucleophilic sites (i.e., O and N atoms) in TMZ, whereas LUMO orbitals were concentrated over the electrophilic regions (i.e., Be and B atoms) of the studied nanocarriers. For TMZ•••nanocarrier complexes, apparent changes were noticed in HOMO and LUMO distributions due to the adsorption of TMZ (Figure 6). It was intriguing to note that the alteration in HOMO and LUMO distributions strongly affirmed the occurrence of the charge transfer within studied complexes, as previously recommended.[53]

From Table 4, intriguing changes were observed in the calculated electronic parameters for $Be_{12}O_{12}$ compared to those for $B_{12}N_{12}$. From numerical data, $E_{HOMO}$ values were found to be −10.60 and −9.54 eV for $Be_{12}O_{12}$ and $B_{12}N_{12}$, while $E_{LUMO}$ = −0.67 and −0.35 eV, respectively.

Table 4. Obtained Values of Electronic Parameters Before and Following the TMZ Adsorption over Nanocarriers[a]

| system | configuration | $E_{HOMO}$ (eV) | $E_{LUMO}$ (eV) | $E_{gap}$ (eV) | $E_{FL}$ (eV) |
|---|---|---|---|---|---|
| TMZ | | −8.52 | −1.63 | 6.89 | −5.07 |
| $Be_{12}O_{12}$ | | −10.60 | −0.67 | 9.93 | −5.63 |
| $B_{12}N_{12}$ | | −9.54 | −0.35 | 9.19 | −4.94 |
| TMZ•••$Be_{12}O_{12}$ | A | −9.00 | −2.15 | 6.85 | −5.57 |
| | B | −9.02 | −2.00 | 7.02 | −5.51 |
| | C | −8.95 | −2.14 | 6.82 | −5.55 |
| | D | −9.00 | −2.44 | 6.55 | −5.72 |
| TMZ•••$B_{12}N_{12}$ | A | −8.36 | −2.53 | 5.84 | −5.44 |
| | B | −8.80 | −2.32 | 6.49 | −5.56 |
| | C | −8.88 | −2.52 | 6.36 | −5.70 |
| | D | −8.66 | −2.89 | 5.77 | −5.77 |

[a]The calculated values are given in eV.

According to the TMZ adsorption, the $E_{HOMO}$, $E_{FL}$, $E_{LUMO}$, and $E_{gap}$ values were significantly changed, demonstrating the influence of TMZ adsorption on the electronic parameters of the nanocarriers. For instance, the $E_{HOMO}$ value for the $Be_{12}O_{12}$ nanocarrier was noticed to be −10.60 eV, while the $E_{HOMO}$ for TMZ•••$Be_{12}O_{12}$ complex within configuration A was −9.00 eV. Moreover, a noticeable decrement was found for $E_{gap}$ values following the adsorption process that modified the conductivity of nanocarriers.[54] Numerically, the $Be_{12}O_{12}$ nanocarrier had an $E_{gap}$ value of 9.93 eV that diminished to 6.85 eV for the TMZ•••$Be_{12}O_{12}$ complex within configuration A. Hence, the adsorption of TMZ leads to a diminution in the values of the energy gap ($E_{gap}$) and a distinct change in the electronic attributes for $Be_{12}O_{12}$ and $B_{12}N_{12}$. In the context of the energy gap, such diminution in $E_{gap}$ leads to an increment in the conductivity, confirming the promising application of $Be_{12}O_{12}$ and $B_{12}N_{12}$ nanocarriers as electrochemical biosensors for the TMZ drug.

**Global Indices of Reactivity.** Toward more reliable insights into electronic parameters, global reactivity descriptors were calculated for the studied monomers and their associated complexes. The obtained values are listed in Table 5.

Table 5 reports considerable differences in global indices of reactivity after the adsorption of TMZ over the surface of the investigated nanocarriers. From the tabulated data, the $Be_{12}O_{12}$ exhibited *EA* with a value of 0.67 eV that changed to 2.15 eV for the TMZ•••$Be_{12}O_{12}$ complex within configuration A. Furthermore, a noticeable alteration was noticed in the *IP* value of the $Be_{12}O_{12}$ from 10.60 to 9.00 eV as a result of TMZ adsorption within configuration A. Interestingly, the feasibility of the adsorption process was confirmed through the


https://doi.org/10.1021/acsomega.4c02882
ACS Omega 2024, 9, 25203−25214

Table 5. Chemical Descriptors for the Optimized TMZ, $Be_{12}O_{12}$, and $B_{12}N_{12}$ Molecules, along with Their Studied Complexes

| system | configuration | *IP* (eV) | *EA* (eV) | $\omega$ (eV) | $\eta$ (eV) | $\mu$ (eV) | *S* ($eV^{-1}$) | $\Phi$ (eV) |
|---|---|---|---|---|---|---|---|---|
| TMZ | | 8.52 | 1.63 | 3.73 | 3.44 | −5.07 | 0.29 | 5.07 |
| $Be_{12}O_{12}$ | | 10.60 | 0.67 | 3.19 | 4.97 | −5.63 | 0.20 | 5.63 |
| $B_{12}N_{12}$ | | 9.54 | 0.35 | 2.66 | 4.60 | −4.94 | 0.22 | 4.94 |
| TMZ•••$Be_{12}O_{12}$ | A | 9.00 | 2.15 | 4.54 | 3.42 | −5.57 | 0.29 | 5.57 |
| | B | 9.02 | 2.00 | 4.33 | 3.51 | −5.51 | 0.28 | 5.51 |
| | C | 8.95 | 2.14 | 4.51 | 3.41 | −5.55 | 0.29 | 5.55 |
| | D | 9.00 | 2.44 | 4.99 | 3.28 | −5.72 | 0.31 | 5.72 |
| TMZ•••$B_{12}N_{12}$ | A | 8.36 | 2.53 | 5.08 | 2.92 | −5.44 | 0.34 | 5.44 |
| | B | 8.80 | 2.32 | 4.77 | 3.24 | −5.56 | 0.31 | 5.56 |
| | C | 8.88 | 2.52 | 5.10 | 3.18 | −5.70 | 0.31 | 5.70 |
| | D | 8.66 | 2.89 | 5.78 | 2.88 | −5.77 | 0.35 | 5.77 |

diminution in $\eta$ and enhancement in *S* values after the adsorption of TMZ over the investigated nanocarriers. To sum up, the differences in the calculated parameters before and following the adsorption confirmed the adsorbing tendency of the studied nanocarriers toward TMZ.

**DOS Analysis.** In an effort to gain further insights into electronic features, the density of state (DOS) analysis was constructed for the studied systems, where total DOS and partial DOS (TDOS and PDOS, respectively) plots were generated. Figure 7 compiles the TDOS plots for isolated

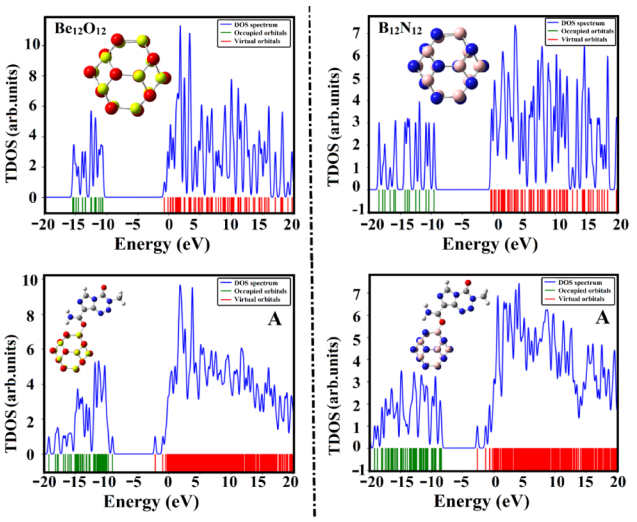


**Figure 7.** Graphed 2D TDOS diagrams for $Be_{12}O_{12}$ and $B_{12}N_{12}$ along with their corresponding complexes with TMZ within configuration A.

$Be_{12}O_{12}$ and $B_{12}N_{12}$, along with their complexes with TMZ drug within configuration A, while plots for the other configurations are collected in Figure S2. Furthermore, PDOS plots are gathered in Figure S3.

As shown in Figures 7 and S2, the adsorption of TMZ over the investigated nanocarriers induced notable changes in the TDOS diagrams. Thus, the TDOS analyses imply that the TMZ interacts effectively with nanocarriers, which is in line with the affirmations of the adsorption energy calculations (Table 1). From PDOS plots, a significant overlap between the $O_s/O_p/N_s/N_p$ orbitals of the TMZ drug and the $Be_s/Be_p/B_s/B_p$ orbitals of nanocarriers was observed (see Figure S3). These observations illustrate the contributions of the *s*- and *p*-orbitals to the occurrence of the adsorption process.

**Solvent Effect.** Inspired by a successful drug delivery process, the vital role of the solvent cannot be neglected. To establish the water effect on the studied adsorption process, adsorption ($E_{ads}^{solvent}$) and solvation ($\Delta E_{solv}$) energies were evaluated (Table 6).

Table 6. Adsorption ($E_{ads}^{solvent}$) and Solvation ($\Delta E_{solv}$) Energies for the Optimized TMZ•••Nanocarrier Complexes[a]

| complex | configuration | $E_{ads}^{solvent}$ (kcal/mol) | $\Delta E_{solv}$ (kcal/mol) |
|---|---|---|---|
| TMZ•••$Be_{12}O_{12}$ | A | −22.26 | −47.53 |
| | B | −19.45 | −48.53 |
| | C | −11.66 | −49.14 |
| | D | −8.88 | −49.50 |
| TMZ•••$B_{12}N_{12}$ | A | −28.05 | −18.15 |
| | B | −25.82 | −18.14 |
| | C | −11.70 | −17.63 |
| | D | −10.96 | −18.25 |

[a] $\Delta E_{solv} = E_{solvent} - E_{gas}$.

From Table 6, the adsorption tendency of studied nanocarriers toward TMZ in the water phase was clearly demonstrated through negative adsorption ($E_{ads}^{solvent}$) energies. Noticeably, configuration A exhibited the most favorable ($E_{ads}^{solvent}$) value than others, and the adsorption energy decreased in the order of A > B > C > D. For instance, $E_{ads}^{solvent}$ was found with values of −22.26, − 19.45, − 11.66, and −8.88 kcal/mol for TMZ•••$Be_{12}O_{12}$ complexes within configurations A, B, C, and D, respectively. Furthermore, negative values of the solvation energy ($E_{solv}$) affirmed the favorable adsorption within the studied complexes in the water phase. To summarize, $Be_{12}O_{12}$ and $B_{12}N_{12}$ would be promising nanocarriers for the TMZ drug delivery process.

**Thermodynamic Parameters.** From a thermodynamic point of view, the nature of the studied adsorption process could be anticipated by performing frequency calculations. Thermodynamic variables, introduced as Gibbs free energy ($\Delta G$), enthalpy ($\Delta H$), and entropy ($\Delta S$) were calculated (kcal/mol) for all studied complexes and are collected in Table 7.

From the data in Table 7, almost all studied complexes exhibited favorable thermodynamic features, demonstrating the adsorption process to be spontaneous and exothermic. For the TMZ•••$Be_{12}O_{12}$ complex within configuration A, $\Delta G$, $\Delta H$, and $\Delta S$ parameters were found with values of −18.66, − 28.88,


https://doi.org/10.1021/acsomega.4c02882
ACS Omega 2024, 9, 25203−25214

**Table 7. Computed Thermodynamic Parameters (kcal/mol) for TMZ•••Nanocarrier Complexes**

| complex | configuration | Δ*G* | Δ*H* | Δ*S* |
|---|---|---|---|---|
| TMZ•••$Be_{12}O_{12}$ | A | −18.66 | −28.88 | −0.043 |
| | B | −15.29 | −25.16 | −0.044 |
| | C | −8.54 | −17.03 | −0.040 |
| | D | −4.89 | −13.54 | −0.041 |
| TMZ•••$B_{12}N_{12}$ | A | −12.00 | −25.35 | −0.039 |
| | B | −9.19 | −23.08 | −0.039 |
| | C | 2.79 | −10.02 | −0.035 |
| | D | 4.29 | −8.11 | −0.033 |

and −0.043 kcal/mol, respectively. Numerically, Δ*G* values for configuration A were found to be −18.66 and −12.00 kcal/mol for TMZ•••$Be_{12}O_{12}$ and •••$B_{12}N_{12}$ complexes, respectively. Indeed, these observations were strongly linked to the data in Table 1, affirming the favorability of the studied drug delivery process.

**Infrared (IR) and Raman Spectra.** The infrared (IR) and Raman spectra are effective tools to characterize chemical systems by identifying the functional groups. The infrared and Raman spectra for the isolated $Be_{12}O_{12}$ and $B_{12}N_{12}$ nanocarriers and their corresponding complexes with TMZ drug were extracted (Figures 8 and S4).

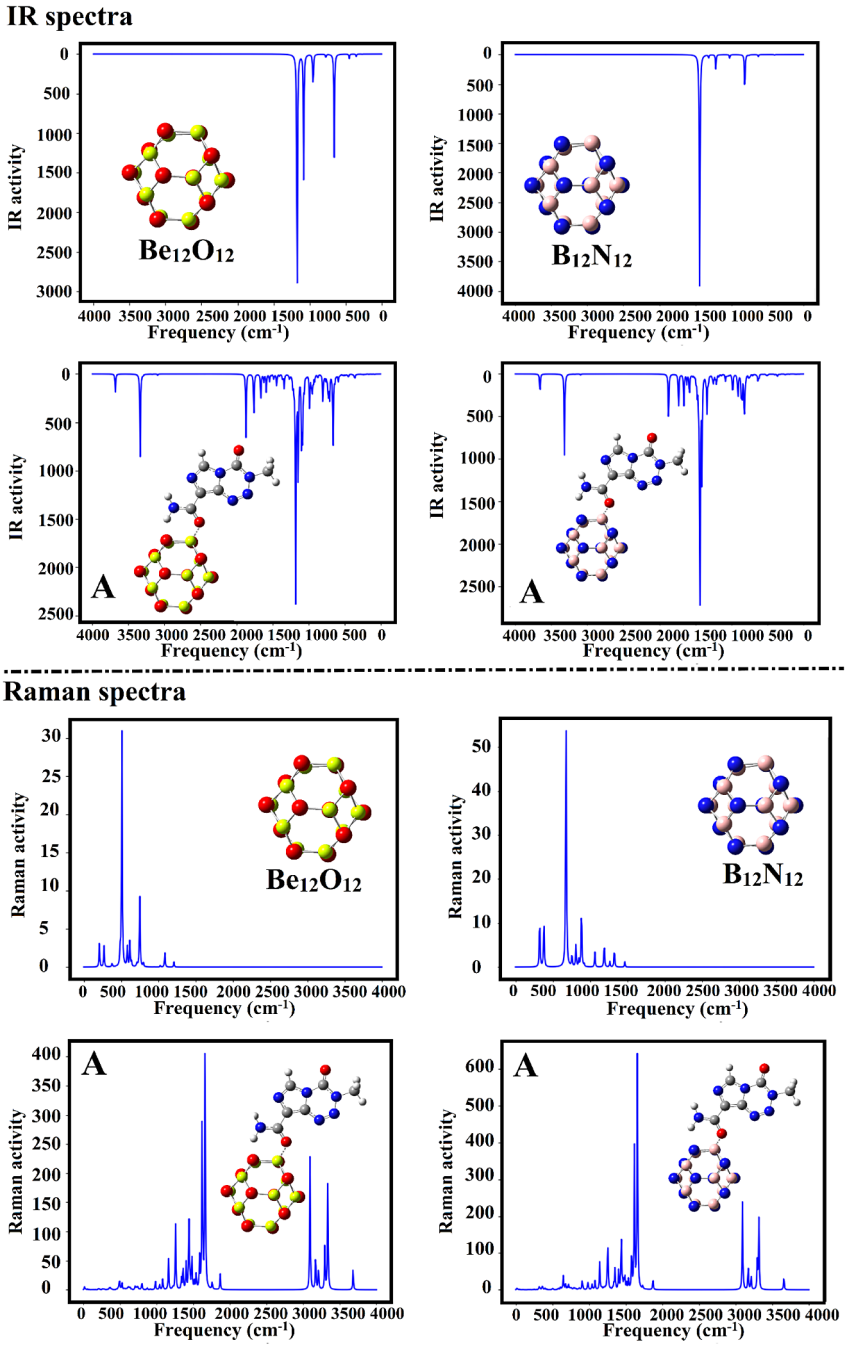


**Figure 8.** Diagrams of infrared (IR) and Raman spectra for the isolated nanocarriers and TMZ•••nanocarrier complexes within configuration A.



https://doi.org/10.1021/acsomega.4c02882
ACS Omega 2024, 9, 25203−25214

Table 8. Recovery Time Values ($\tau$, in $\mu$s) for the TMZ•••Nanocarrier Complexes

| complex | configuration | T (298.15 K) | T (310.15 K) | T (315.15 K) |
|---|---|---|---|---|
| TMZ•••$Be_{12}O_{12}$ | A | $4.56 \times 10$ | $1.35 \times 10$ | 8.35 |
| | B | $1.58 \times 10^{-1}$ | $5.74 \times 10^{-2}$ | $3.87 \times 10^{-2}$ |
| | C | $1.78 \times 10^{-6}$ | $1.02 \times 10^{-6}$ | $8.20 \times 10^{-7}$ |
| | D | $3.80 \times 10^{-9}$ | $2.76 \times 10^{-9}$ | $2.43 \times 10^{-9}$ |
| TMZ•••$B_{12}N_{12}$ | A | $6.08 \times 10^{-4}$ | $2.78 \times 10^{-4}$ | $2.04 \times 10^{-4}$ |
| | B | $5.33 \times 10^{-6}$ | $2.93 \times 10^{-6}$ | $2.31 \times 10^{-6}$ |
| | C | $9.07 \times 10^{-15}$ | $1.09 \times 10^{-14}$ | $1.17 \times 10^{-14}$ |
| | D | $7.24 \times 10^{-16}$ | $9.58 \times 10^{-16}$ | $7.24 \times 10^{-16}$ |

Table 9. Optimum Distance (Å) and Energetic Values along with Thermodynamic Parameters for the Optimized TMZ•••Doped Nanocarrier Complexes (Given in kcal/mol)

| system | configuration | d | $E_{ads}$ | $\Delta G$ | $\Delta H$ | $\Delta S$ |
|---|---|---|---|---|---|---|
| TMZ•••$MgBe_{11}O_{12}$ | A | 1.98 | −42.72 | −28.84 | −41.13 | −0.041 |
| | B | 2.09 | −33.78 | −19.71 | −32.17 | −0.042 |
| | C | 1.99 | −28.39 | −17.70 | −27.07 | −0.039 |
| | D | 2.17 | −23.20 | −10.49 | −21.64 | −0.037 |
| TMZ•••$AlB_{11}N_{12}$ | A | 1.83 | −60.55 | −45.53 | −58.74 | −0.044 |
| | B | 1.95 | −49.91 | −34.98 | −48.16 | −0.044 |
| | C | 1.85 | −42.33 | −28.98 | −40.98 | −0.040 |
| | D | 2.02 | −35.23 | −21.32 | −33.51 | −0.041 |

From Figures 8 and S4, the IR spectra revealed apparent alterations in the stretching bands of the $Be_{12}O_{12}$ and $B_{12}N_{12}$ nanocarriers after TMZ adsorption. Additionally, new peaks were observed for the TMZ•••$Be_{12}O_{12}$ and •••$B_{12}N_{12}$ complexes, ensuring favorability of the studied adsorption process. Thence, significant changes were found in the Raman spectra. These alterations highlighted the suitability of $Be_{12}O_{12}$ and $B_{12}N_{12}$ nanocarriers to be engaged in the delivery of TMZ.

**Recovery Time.** To systematically consider the drug delivery process, the desorption process must be assumed for the studied complexes. Thus, the recovery time ($\tau$) was calculated for all studied TMZ•••$Be_{12}O_{12}$ and •••$B_{12}N_{12}$ complexes to determine the difficulty of releasing the drug toward the intended target site. Herein, recovery time ($\tau$) values were computed by applying different temperatures (Table 8).

Table 8 indicates that the recovery time ($\tau$) values were associated with adsorption energy values; as the adsorption energy increased, the recovery time increased. Numerically, TMZ•••$Be_{12}O_{12}$ complex within configuration A exhibited the most negative adsorption energy ($E_{ads}$ = −30.47 kcal/mol) and the longest recovery ($\tau$) time of $4.56 \times 10$ $\mu$s at room temperature. Furthermore, a noticeable decrease in recovery time ($\tau$) values was indicated as the temperature increased. For TMZ•••$B_{12}N_{12}$ complex in configuration A, as an example, the $\tau$ values were $6.08 \times 10^{-4}$, $2.78 \times 10^{-4}$, and $2.04 \times 10^{-4}$ $\mu$s at room, human body, and cancer cell temperatures, respectively. According to the obtained data, $Be_{12}O_{12}$ and $B_{12}N_{12}$ would be potent nanocarriers for the TMZ drug delivery process.

**Doping Effect.** The potential aspects of the doping process on the delivery of different drugs were amply demonstrated by the literature.[55,56] Thus, the doping process was applied to TMZ•••nanocarrier adsorption using Al and Mg atoms to form $AlB_{11}N_{12}$ and $MgBe_{11}O_{12}$ nanocarriers, respectively. Consequently, ESP analyses for the doped nanocarriers were executed and are listed in Figure S5. Geometrical optimization as well as energy calculations were performed for TMZ•••$MgBe_{11}O_{12}$ and •••$AlB_{11}N_{12}$ complexes within the selected A↔D configurations (Figure S6 and Table 9). Furthermore, IR and Raman spectra were generated for doped nanocarriers along with TMZ•••doped nanocarrier complexes (Figure S7).

Figure S5 obviously displays the effect of doping on the geometrical characteristics (i.e., bond length and bond angle) of the studied nanocarriers. As a consequence, the Mg−O and Al−N bond lengths were found to be 1.87 and 1.78 Å for $MgBe_{11}O_{12}$ and $AlB_{11}N_{12}$, respectively. Thus, a substantial elongation in bond lengths was found as a result of the doping process (Figure 2), which is in line with the literature.[57]

According to Figure S5, the electrophilic nature of doped nanocarriers was found to be more than pure analogs. The $V_{s,max}$ values over the doped atoms were noticed to be 242.2 and 158.9 kcal/mol in the $MgBe_{11}O_{12}$ and $AlB_{11}N_{12}$ nanocarriers, respectively. Furthermore, the negative values of $V_{s,min}$ around the O and N atoms of $MgB_{11}O_{12}$ and $AlB_{11}N_{12}$ nanocarriers were found to be −31.6 and −20.2 kcal/mol, respectively. Illustratively, the adsorption process of TMZ drug over doped nanocarriers was proposed to be more favorable.

For the targeted drug delivery process, geometrical optimization was performed for the TMZ•••$MgBe_{11}O_{12}$ and •••$AlB_{11}N_{12}$ complexes. For the optimized complexes, the adsorption energies and thermodynamic parameters were calculated (Table 9).

From Table 9 and Figure S6 significant adsorption energy values were noticed for all studied complexes, demonstrating the enhancing role of Mg- and Al-doped atoms in the adsorption process. Similar to the data in Table 1, configuration A exhibited the most negative $E_{ads}$ value, compared to the other configurations B↔D. According to thermodynamic parameters, the exothermic and spontaneous natures were approved for all studied complexes. Numerically, $\Delta G$, $\Delta H$, and $\Delta S$ parameters for the TMZ•••$MgBe_{11}O_{12}$ complex were found to be −28.84, − 41.13, and −0.041 kcal/mol within configuration A, respectively. From Figure S7, obvious changes in the IR and Raman spectra of $MgBe_{11}O_{12}$


https://doi.org/10.1021/acsomega.4c02882
ACS Omega 2024, 9, 25203−25214

and $AlB_{11}N_{12}$ nanocarriers were found following the adsorption of TMZ. Furthermore, new peaks were observed for the TMZ•••$MgBe_{11}O_{12}$ and •••$AlB_{11}N_{12}$ complexes, confirming the occurrence of the investigated adsorption process. Inspired by the above-mentioned data, the doping process by Mg and Al atoms for $Be_{12}O_{12}$ and $B_{12}N_{12}$ nanocarriers played an enhancing role in the adsorption process.

## CONCLUSION

The adsorption behavior of $Be_{12}O_{12}$ and $B_{12}N_{12}$ nanocarriers toward the temozolomide (TMZ) anticancer drug was investigated by DFT calculations. Toward the adsorption process, TMZ interacted with $Be_{12}O_{12}$ and $B_{12}N_{12}$ via four nucleophilic sites (configurations A↔D). According to ESP results, the electrophilic and nucleophilic natures were illustrated for nanocarriers and TMZ, respectively. For the adsorption phenomena, negative adsorption energies demonstrated the favorable tendency of $Be_{12}O_{12}$ and $B_{12}N_{12}$ to adsorb TMZ within different orientations. The adsorption energy for configuration A was found to exhibit the most negative value among all of the studied configurations. Within SAPT analysis, the adsorption process was found to be strongly controlled with electrostatic force, followed by dispersion and induction forces. From an electronic perspective, the distributions of FMOs (HOMO and LUMO) were changed after the adsorption of TMZ, demonstrating the occurrence of the adsorption process. From a thermodynamic point of view, the nature of the considered adsorption process within all studied complexes was documented as spontaneous and exothermic. In the context of water, a favorable adsorption process was noticed within all studied configurations through negative $E_{ads}^{solvent}$ and $E_{solv}$ values. Eventually, substantial recovery time values were observed for all studied complexes, demonstrating the tendency of TMZ to separate from the nanocarriers. From a comparative point of view, the adsorption of TMZ over doped nanocarriers (i.e., $MgB_{11}O_{12}$ and $AlB_{11}N_{12}$) was more favorable than that of pure counterparts (i.e., $Be_{12}O_{12}$ and $B_{12}N_{12}$). Accordingly, the doping process had a favorable impact on the TMZ adsorption process. The outcomes aimed to introduce an effective nanocarrier to be applied in the drug delivery process.

## ASSOCIATED CONTENT

### Supporting Information

The Supporting Information is available free of charge at https://pubs.acs.org/doi/10.1021/acsomega.4c02882.

2D Noncovalent interaction (NCI) plots, TDOS plots, PDOS plots, and IR and Raman spectra for the optimized TMZ•••nanocarrier complexes; the optimized structures and IR and Raman spectra for doped nanocarriers and TMZ•••doped nanocarrier complexes; and Cartesian atomic coordinates for pure and dopped nanocarriers (PDF)

## AUTHOR INFORMATION


### Corresponding Authors

**Mahmoud A. A. Ibrahim** − *Computational Chemistry Laboratory, Chemistry Department, Faculty of Science, Minia University, Minia 61519, Egypt; School of Health Sciences, University of KwaZulu-Natal, Westville Campus, Durban 4000, South Africa;* orcid.org/0000-0003-4819-2040; Email: m.ibrahim@compchem.net

**Tamer Shoeib** − *Department of Chemistry, The American University in Cairo, New Cairo 11835, Egypt;* orcid.org/0000-0003-3512-1593; Email: t.shoeib@aucegypt.edu

### Authors

**Al-Shimaa S. M. Rady** − *Computational Chemistry Laboratory, Chemistry Department, Faculty of Science, Minia University, Minia 61519, Egypt*

**Peter A. Sidhom** − *Department of Pharmaceutical Chemistry, Faculty of Pharmacy, Tanta University, Tanta 31527, Egypt;* orcid.org/0000-0003-2579-6351

**Shaban R. M. Sayed** − *Department of Botany and Microbiology, College of Science, King Saud University, Riyadh 11451, Saudi Arabia*

**Khalid Elfaki Ibrahim** − *Department of Zoology, College of Science, King Saud University, Riyadh 11451, Saudi Arabia*

**Ahmed M. Awad** − *Department of Chemistry, California State University Channel Islands, Camarillo, California 93012, United States;* orcid.org/0000-0002-6991-9336

**Lamiaa A. Mohamed** − *Computational Chemistry Laboratory, Chemistry Department, Faculty of Science, Minia University, Minia 61519, Egypt*

Complete contact information is available at: https://pubs.acs.org/10.1021/acsomega.4c02882


### Author Contributions

M.A.A.I. contributed to conceptualization, methodology, software, resources, project administration, supervision, and writing—review and editing. A.-s.S.M.R. contributed to formal analysis, methodology, investigation, data curation, writing—original draft, and visualization. PA.S. contributed to visualization and writing—review and editing. S.R.M.S. contributed to resources and writing—review and editing. K.E.I. contributed to resources and writing—review and editing. A.M.A. contributed to visualization and writing—review and editing. Tamer Shoeib contributed to conceptualization, project administration, resources, and writing—review and editing. L.A.M. contributed to formal analysis, methodology, investigation, software, visualization, and writing—review and editing. All authors have read and agreed to the published version of the manuscript.

### Notes

The authors declare no competing financial interest.

## ACKNOWLEDGMENTS

The authors extend their appreciation to the Researchers Supporting Project number (RSPD2024R759), King Saud University, Riyadh, Saudi Arabia, for funding this work. The computational work was completed with resources provided by the Center for High-Performance Computing (Cape Town, South Africa, http://www.chpc.ac.za), Bibliotheca Alexandrina (http://hpc.bibalex.org), and the American University in Cairo.

## REFERENCES

(1) Bangham, A. D.; Standish, M. M.; Watkins, J. C. Diffusion of univalent ions across the lamellae of swollen phospholipids. *J. Mol. Biol.* **1965**, *13*, 238−252.

(2) Chatterjee, P.; Kumar, S. Current developments in nanotechnology for cancer treatment. *Mater. Today: proc.* **2022**, *48*, 1754−1758.

(3) Petranovska, A. L.; Abramov, N. V.; Turanska, S. P.; Gorbyk, P. P.; Kaminskiy, A. N.; Kusyak, N. V. Adsorption of cis-

dichlorodiammineplatinum by nanostructures based on single-domain magnetite. *J. Nanostructure Chem.* **2015**, *5*, 275−285.
(4) Tiwari, P. M.; Vig, K.; Dennis, V. A.; Singh, S. R. Functionalized gold nanoparticles and their biomedical applications. *Nanomater* **2011**, *1*, 31−63.
(5) Ohta, T.; Hashida, Y.; Yamashita, F.; Hashida, M. Development of novel drug and gene delivery carriers composed of single-walled carbon nanotubes and designed peptides with pegylation. *J. Pharm. Sci.* **2016**, *105*, 2815−2824.
(6) Amna, T.; Hassan, M. S.; Gharsan, F. N.; Rehman, S.; Sheikh, F. A. Nanotechnology in drug delivery systems: Ways to boost bioavailability of drugs. In *Nanotechnology for Infectious Diseases*; Springer, 2022; pp. 223236.
(7) Ibrahim, M. A. A.; Hamad, M. H. A.; Mahmoud, A. H. M.; Mekhemer, G. A. H.; Sayed, S. R. M.; El-Rahman, M. K. A.; Sidhom, P. A.; Dabbish, E.; Shoeib, T. On the use of graphene nanosheets for drug delivery: A case study of cisplatin and some of its analogs. *Pharmaceutics* **2023**, *15*, 1640.
(8) Hamimed, S.; Jabberi, M.; Chatti, A. Nanotechnology in drug and gene delivery. *Naunyn Schmiedebergs Arch. Pharmacol.* **2022**, *395*, 769−787.
(9) Rady, A. S. M.; Moussa, N. A. M.; Mohamed, L. A.; Sidhom, P. A.; Sayed, S. R. M.; Abd El-Rahman, M. K.; Dabbish, E.; Shoeib, T.; Ibrahim, M. A. A. Elucidating the adsorption of 2-Mercaptopyridine drug on the aluminum phosphide (Al(12)P(12)) nanocage: A DFT study. *Heliyon* **2023**, *9*, No. e18690.
(10) Kobylinska, L.; Mitina, N.; Zaichenko, A.; Stoika, R. Controlled delivery and reduced side effects of anticancer drugs complexed with polymeric nanocarrier. In *Biomedical Nanomaterials*, Stoika, R. S. Eds.; Springer International Publishing: Cham, 2022; pp. 119147.
(11) Sozer, S. C.; Akdogan, Y. Characterization of water solubility and binding of spin labeled drugs in the presence of albumin nanoparticles and proteins by electron paramagnetic resonance spectroscopy. *ChemistrySelect* **2022**, *7*, No. e202103890.
(12) Li, S. D.; Huang, L. Pharmacokinetics and biodistribution of nanoparticles. *Mol. Pharm.* **2008**, *5*, 496−504.
(13) Ciofani, G.; Danti, S.; Genchi, G. G.; Mazzolai, B.; Mattoli, V. Boron nitride nanotubes: biocompatibility and potential spill-over in nanomedicine. *Small* **2013**, *9*, 1672−1685.
(14) Mateti, S.; Wong, C. S.; Liu, Z.; Yang, W. R.; Li, Y. C.; Li, L. H.; Chen, Y. Biocompatibility of boron nitride nanosheets. *Nano Res.* **2018**, *11*, 334−342.
(15) Yousefi, M.; Rad, M. S.; Shakibazadeh, R.; Ghodrati, L.; Kachoie, M. A. Simulating a heteroatomic CBN fullerene-like nanocage towards the drug delivery of fluorouracil. *Mol. Simul.* **2022**, *48*, 1284−1292.
(16) Giannopoulos, G. I. Fullerene Derivatives for Drug Delivery against COVID-19: A Molecular Dynamics Investigation of Dendro[60]fullerene as Nanocarrier of Molnupiravir. *Nanomater* **2022**, *12*, 2711.
(17) Rezaei-Sameti, M.; Abdoli, S. K. The capability of the pristine and (Sc, Ti) doped $Be_{12}O_{12}$ nanocluster to detect and adsorb of Mercaptopyridine molecule: A first principle study. *J. Mol. Struct.* **2020**, *1205*, 127593.
(18) Wu, S.; Li, L.; Liang, Q.; Gao, H.; Tang, T.; Tang, Y. A DFT study of sulforaphane adsorbed on M12O12(M = Be, Mg and Ca) nanocages. *Mater. Today Commun.* **2024**, *38*, 107687.
(19) Yao, C.; Xiang, F.; Xu, Z. Metal oxide nanocage as drug delivery systems for Favipiravir, as an effective drug for the treatment of COVID-19: a computational study. *J. Mol. Model.* **2022**, *28*, 64.
(20) Ma, S.; Yi, L.; Wu, Z. Metal oxide (BeO-MgO-ZnO) nanoclusters as drug delivery systems for isoniazid anticancer drug: a DFT study. *Mol. Phys.* **2022**, *120* (3), No. e1986162.
(21) Al-Otaibi, J. S.; Mary, Y. S.; Mary, Y. S.; Mondal, A.; Acharjee, N.; Rajendran Nair, D. S. Investigation of the interaction of thymine drugs with Be(12)O(12) and Ca(12)O(12) nanocages: A quantum chemical study. *Spectrochim. Acta, Part A* **2024**, *308*, 123728.
(22) Al-Otaibi, J. S.; Alamro, F. S.; Almugrin, A. H.; Mary, Y. S.; Mary, Y. S.; Rajendran Nair, D. S. Revealing patterns in Be12O12-metal nanocages as a nitrosourea drug delivery system: DFT, SERS, solvent effects and the role of periods and groups. *Comput. Theor. Chem.* **2024**, *1236*, 114604.
(23) Javan, M. B.; Soltani, A.; Azmoodeh, Z.; Abdolahi, N.; Gholami, N. A DFT study on the interaction between 5-fluorouracil and B12N12 nanocluster. *RSC Adv.* **2016**, *6*, 104513−104521.
(24) Seifert, G.; Fowler, P. W.; Mitchell, D.; Porezag, D.; Frauenheim, T. Boron-nitrogen analogues of the fullerenes: Electronic and structural properties. *Chem. Phys. Lett.* **1997**, *268*, 352−358.
(25) Chen, X.; Wu, P.; Rousseas, M.; Okawa, D.; Gartner, Z.; Zettl, A.; Bertozzi, C. R. Boron nitride nanotubes are noncytotoxic and can be functionalized for interaction with proteins and cells. *J. Am. Chem. Soc.* **2009**, *131*, 890−891.
(26) Jensen, F.; Toftlund, H. Structure and stability of C24 and B12n12 isomers. *Chem. Phys. Lett.* **1993**, *201*, 89−96.
(27) Ibrahim, M. A. A.; Rady, A.-S. S. M.; Moussa, N. A. M.; Ahmed, M. N.; Sidhom, P. A.; Shawky, A. M.; Alqahtani, A. M.; Mohamed, L. A. Investigation of aluminum nitride nanocarrier for drug delivery process of Favipiravir: A DFT study. *J. Mol. Liq.* **2023**, *372*, 121209.
(28) Ibrahim, M. A. A.; Rady, A. S. M.; Mohamed, L. A.; Shawky, A. M.; Hasanin, T. H. A.; Sidhom, P. A.; Moussa, N. A. M. Adsorption of Molnupiravir anti-COVID-19 drug over B(12)N(12) and Al(12)-N(12) nanocarriers: a DFT study. *J. Biomol. Struct. Dyn.* **2023**, 1−15.
(29) Celaya, C. A.; Hernández-Ayala, L. F.; Zamudio, F. B.; Vargas, J. A.; Reina, M. Adsorption of melphalan anticancer drug on C, BN, BCN, CN and BCN nanocages: A comparative DFT study. *J. Mol. Liq.* **2021**, *329*, 115528.
(30) Kang, D.; Yu, X.; Ge, M.; Xiao, F.; Xu, H. Novel Al-doped carbon nanotubes with adsorption and coagulation promotion for organic pollutant removal. *J. Environ. Sci.* **2017**, *54*, 1−12.
(31) Bibi, S.; Ur-Rehman, S.; Khalid, L.; Bhatti, I. A.; Bhatti, H. N.; Iqbal, J.; Bai, F. Q.; Zhang, H. X. Investigation of the adsorption properties of gemcitabine anticancer drug with metal-doped boron nitride fullerenes as a drug-delivery carrier: a DFT study. *RSC Adv.* **2022**, *12*, 2873−2887.
(32) Hazrati, M. K.; Javanshir, Z.; Bagheri, Z. B24N24 fullerene as a carrier for 5-fluorouracil anti-cancer drug delivery: DFT studies. *J. Mol. Graph Model.* **2017**, *77*, 17−24.
(33) Golipour-Chobar, E.; Salimi, F.; Rajaei, G. E. Boron nitride nanocluster as a carrier for lomustine anticancer drug delivery: DFT and thermodynamics studies. *Monatsh. Chem.* **2020**, *151* (3), 309−318.
(34) Zhu, H.; Zhao, C. F.; Cai, Q. H.; Fu, X. M.; Sheykhahmad, F. R. Adsorption behavior of 5-aminosalicylic acid drug on the BN, AlBN and GaBN nanoclusters: A comparative DFT study. *Inorg. Chem. Commun.* **2020**, *114*, 107808.
(35) Ibrahim, M. A. A.; Rady, A. S. M.; Mandarawe, A. M. A.; Mohamed, L. A.; Shawky, A. M.; Hasanin, T. H. A.; Sidhom, P. A.; Soliman, M. E. S.; Moussa, N. A. M. Adsorption of chlormethine anticancer drug on pure and aluminum-doped boron nitride nanocarriers: A comparative DFT study. *Pharmaceuticals* **2022**, *15*, 1181.
(36) Stupp, R.; Hegi, M. E.; Mason, W. P.; van den Bent, M. J.; Taphoorn, M. J.; Janzer, R. C.; Ludwin, S. K.; Allgeier, A.; Fisher, B.; Belanger, K.; et al. European Organisation for, R.; Treatment of Cancer Brain, T.; Radiation Oncology, G.; National Cancer Institute of Canada Clinical Trials, G., Effects of radiotherapy with concomitant and adjuvant Temozolomide versus radiotherapy alone on survival in glioblastoma in a randomised phase III study: 5-year analysis of the EORTC-NCIC trial. *Lancet Oncol.* **2009**, *10*, 459−466.
(37) Yang, J.; Xu, Y.; Fu, Z.; Chen, J.; Fan, W.; Wu, X. Progress in research and development of Temozolomide brain-targeted preparations: a review. *J. Drug Target.* **2023**, *31*, 119−133.
(38) Ndjopme Wandji, B. L.; Tamafo Fouegue, A. D.; Nkungli, N. K.; Ntieche, R. A.; Wahabou, A. DFT investigation on the application of pure and doped X(12)N(12) (X = B and Al) fullerene-like nanocages toward the adsorption of Temozolomide. *R Soc. Open Sci.* **2022**, *9*, 211650.
(39) Tamafo Fouegue, A. D.; de Paul Zoua, V.; Kounou, G. N.; Ndjopme Wandji, B. L.; Ghogomu, J. N.; Ntieche, R. A. DFT


https://doi.org/10.1021/acsomega.4c02882
*ACS Omega* 2024, 9, 25203−25214

investigation of Temozolomide drug delivery by pure and boron doped C(24) fullerene-like nanocages. *Nanoscale Adv.* **2023**, *5*, 5880−5891.
(40) Frisch, J.; T, G. W.; Schlegel, H. B.; Scuseria, G. E.; Robb, M. A.; Cheeseman, J. R.; Scalmani, G.; Barone, V.; Mennucci, B.; Petersson, G. A., et al. Wallingford CT: Gaussian, Inc.; 2009.
(41) Zhao, Y.; Truhlar, D. G. The M06 suite of density functionals for main group thermochemistry, thermochemical kinetics, noncovalent interactions, excited states, and transition elements: two new functionals and systematic testing of four M06-class functionals and 12 other functionals. *Theor. Chem. Acc.* **2008**, *120*, 215−241.
(42) Ibrahim, M. A. A. Molecular mechanical perspective on halogen bonding. *J. Mol. Model.* **2012**, *18*, 4625−4638.
(43) Lu, T.; Chen, F. Multiwfn: a multifunctional wavefunction analyzer. *J. Comput. Chem.* **2012**, *33*, 580−592.
(44) Gutowski, M.; Vanduijneveldtvanderijdt, G. C.; Vanlenthe, J. H.; Vanduijneveldt, F. B. Accuracy of the boys and bernardi function counterpoise method. *J. Chem. Phys.* **1993**, *98*, 4728−4738.
(45) Parrish, R. M.; Burns, L. A.; Smith, D. G. A.; Simmonett, A. C.; DePrince, A. E., 3rd; Hohenstein, E. G.; Bozkaya, U.; Sokolov, A. Y.; Di Remigio, R.; Richard, R. M.; Gonthier, J. F.; James, A. M.; McAlexander, H. R.; Kumar, A.; Saitow, M.; Wang, X.; Pritchard, B. P.; Verma, P.; Schaefer, H. F., 3rd; Patkowski, K.; King, R. A.; Valeev, E. F.; Evangelista, F. A.; Turney, J. M.; Crawford, T. D.; Sherrill, C. D. Psi4 1.1: An open-source electronic structure program emphasizing automation, advanced libraries, and interoperability. *J. Chem. Theory Comput.* **2017**, *13* (7), 3185−3197.
(46) Humphrey, W.; Dalke, A.; Schulten, K. VMD: Visual molecular dynamics. *J. Mol. Graph.* **1996**, *14*, 33−38.
(47) O'Boyle, N. M.; Tenderholt, A. L.; Langner, K. M. cclib: a library for package-independent computational chemistry algorithms. *J. Comput. Chem.* **2008**, *29*, 839−845.
(48) Esfandiarpour, R.; Badalkhani-Khamseh, F.; Hadipour, N. L. Theoretical studies of phosphorene as a drug delivery nanocarrier for fluorouracil. *RSC Adv.* **2023**, *13*, 18058−18069.
(49) Baei, M. T.; Taghartapeh, M. R.; Lemeski, E. T.; Soltani, A. A computational study of adenine, uracil, and cytosine adsorption upon AlN and BN nano-cages. *Phys. B Condens. Matter.* **2014**, *444*, 6−13.
(50) Hasan, M. M.; Das, A. C.; Hossain, M. R.; Hossain, M. K.; Hossain, M. A.; Neher, B.; Ahmed, F. The computational quantum mechanical investigation of the functionalized boron nitride nanocage as the smart carriers for favipiravir drug delivery: a DFT and QTAIM analysis. *J. Biomol. Struct. Dyn.* **2022**, *40*, 13190−13206.
(51) Afzal, S.; Afzal., F; Ayub, A. R.; Arshed, S.M.; Nabat, K. Y.; Taj, A.; Hamid, H.; Iqbal, J A DFT-Based quantum analysis of Optimizing B3O3 as a melphalan nanocarrier for cancer therapy. *Comput. Theor. Chem.* **2024**, *1236*, 114582.
(52) Souza Macedo, V.; Soares Silva, T.; Guimarães Miranda, T.; Henrique Pereira, D. Assessment of the nanodelivery capacity of antineoplastic jacaranone by B12N12 nanocages: A DFT study. *Comput. Theor. Chem.* **2024**, *1232*, 114461.
(53) Tariq, A.; Nazir, S.; Arshad, A. W.; Nawaz, F.; Ayub, K.; Iqbal, J. DFT study of the therapeutic potential of phosphorene as a new drug-delivery system to treat cancer. *RSC Adv.* **2019**, *9*, 24325−24332.
(54) Afahanam, L. E.; Louis, H.; Benjamin, I.; Gber, T. E.; Ikot, I. J.; Manicum, A. E. Heteroatom (B, N, P, and S)-doped cyclodextrin as a hydroxyurea (HU) drug nanocarrier: A computational approach. *ACS Omega* **2023**, *8*, 9861−9872.
(55) Apebende, C. G.; Ogunwale, G. J.; Louis, H.; Benjamin, I.; Kadiri, M. T.; Owen, A. E.; Manicum, A.-L. E. Density functional theory (DFT) computation of pristine and metal-doped MC59 (M = Au, Hf, Hg, Ir) fullerenes as nitrosourea drug delivery systems. *Mater. Sci. Semicond. Process.* **2023**, *158*, 107362.
(56) Hosseinzadeh, E.; Foroumadi, A.; Firoozpour, L. A DFT study on the transition metal doped BN and AlN nanocages as a drug delivery vehicle for the cladribine drug. *J. Mol. Liq.* **2023**, *374*, 121262.
(57) Zhu, H.; Zhao, C.; Cai, Q.; Fu, X.; Sheykhahmad, F. R. Adsorption behavior of 5-aminosalicylic acid drug on the B12N12, AlB11N12 and GaB11N12 nanoclusters: A comparative DFT study. *Inorg. Chem. Commun.* **2020**, *114*, 107808.


https://doi.org/10.1021/acsomega.4c02882
*ACS Omega* 2024, 9, 25203−25214